Fluorinated PLGA Nanoparticles for Enhanced Drug Encapsulation and 19F NMR Detection

Fluorinated PLGA Nanoparticles for Enhanced Drug Encapsulation and ^{19}F NMR detection

Giulia Neri,[†] *Giuliana Mion,*[†] *Andrea Pizzi*[†] *Linda Chaabane,*[⌋] *Francesco Cellesi*[┼] *Floryan De Campo,*[⊥] *Michele R. Chierotti,*[┤] *Roberto Gobetto,*[┤] *Min Li,*[⌐] *Piergiorgio Messa,*[⌐] *Pierangelo Metrangolo,*[†]* *and Francesca Baldelli Bombelli*[†]*

[†]Laboratory of Supramolecular and Bio-Nanomaterials (SupraBioNanoLab),Department of Chemistry, Materials, and Chemical Engineering "Giulio Natta", Politecnico di Milano, 20131 Milan, Italy;

[⌋] Institute of Experimental Neurology (INSPE) and Experimental Imaging Center (CIS), IRCCS Ospedale San Raffaele, 20132 Milan, Italy;

[┼]Department of Chemistry, Materials, and Chemical Engineering "Giulio Natta", Politecnico di Milano, 20131 Milan, Italy;

[┤]Department of Chemistry and NIS Centre, Università di Torino, 10125 Turin, Italy;

[⌐] Renal Research Laboratory, Fondazione IRCCS Ca' Granda Ospedale Maggiore Policlinico, 20122 Milan, Italy.

[⊥]Solvay Specialty Polymers, Bollate, 20021 Milan, Italy.

KEYWORDS: PLGA, nanoparticles, drug encapsulation, ^{19}F-NMR, theranostic

ABSTRACT. In the continuous search to develop multimodal systems able to show diagnostic and therapeutic combined actions, several efforts are moving toward the development of nanoparticles (NPs). In this context, Magnetic Resonance Imaging (MRI), a non-invasive technique characterized by a high penetration and high spatial resolution, represents a very promising tool. ^{19}F is a good tracer for MRI applications due to its high sensitivity and to low fluorine background signal *in vivo*. Suitable functionalized Poly(lactic-co-glycolic acid) (PLGA) NPs are extensively employed to design multimodal systems due to the exceptional properties of this FDA approved polymer.

Herein we designed, by a covalent approach, a novel class of multifunctional fluorinated co-polymers (F-PLGA) containing an increasing number of fluorine atoms. The self-assembly ability of these fluorinated compounds to give rise to F-PLGA NP derivates able to function both as ^{19}F-NMR probes and as drug carriers was investigated. Finally, the absence of cytotoxicity and a controlled drug release were demonstrated.

Over the last few decades, multimodal polymer NPs have been extensively investigated in medicine with the objective to combine diagnostic and therapeutic functions in the same particle [1]. The FDA approved PLGA is among the most attractive polymeric material for biomedical applications thanks to its high biocompatibility and biodegradability, long-term storage stability and ability to encapsulate and protect drugs by *in vivo* fast degradation [2-5]. In fact, time releases of the encapsulated cargoes from the NPs can be fine-tuned by modulating polymer composition and structural modifications [6].

In the last decades, several multimodal PLGA NPs have been developed through its combination with various imaging techniques, such as magnetic resonance imaging (MRI) [7], ultrasound (US)

[8] and optical imaging (OI) [9]. Among available non-invasive imaging techniques, the potential of ^{19}F MRI has recently emerged thanks to the high natural abundance of ^{19}F nucleus, its high gyromagnetic ratio and its null *in vivo* detectable background due to the virtual absence of organic fluorine in living systems [10,11]. The sensitivity of the ^{19}F nucleus is several orders of magnitude higher than that of ^{13}C and ^{23}Na and comparable to that of the ^{1}H nucleus [12]. This results in a high specificity of the ^{19}F MRI image and in the possibility to directly quantify the signal and the amount of ^{19}F by the data images [13], with a consequent use of ^{19}F probes for *in vivo* tracking [14,15]. Ideal requirement for highly sensitive ^{19}F MRI probes for clinical use is being biocompatible and bearing a high number of magnetically equivalent ^{19}F atoms. Currently, the most used fluorinated contrast agents (CAs) for *in vivo* non-invasive imaging are emulsions of small perfluorinated molecules (PFC) [16] and polymer mixtures of linear perfluoropolyethers (PFPE) [17], mostly used for an efficient *ex vivo* cells labelling without the use of transfection reagents [18,19]. Covalent functionalization of biocompatible materials with suitable fluorinated ligands can also be an interesting strategy to produce probes that do not need further additives for aqueous formulations [20-23]. Critical to the development of an effective ^{19}F NMR probe is to facilitate the mobility of the fluorinated chains, in order to achieve the necessary transverse relaxation time (T_2) for a good signal image [24]. In this sense the use of short and branched fluorinated ligands is preferable to the counterpart linear chains, also in terms of biodistribution and bioaccumulation [25].

Here we reported a covalent strategy to directly functionalize PLGA with a highly mobile fluorinated group to be active in ^{19}F NMR without impacting on its self-assembly ability. PLGA co-polymer has been functionalized with two different fluorinated amine ligands, which contain three and nine equivalent fluorine atoms, respectively. Thus, two novel compounds, F_3-PLGA and

F_9-PLGA, for which synthesis and chemical structure are reported in **Figure 1A**, were obtained. The chemical structure and thermal stability were analysed by solution NMR, DSC and TGA. Moreover, the ability of F_9-PLGA NPs to function both as ^{19}F-NMR probes and drug carriers was also investigated. Thus, dexamethasone (DEX), a synthetic steroidal anti-inflammatory drug containing one fluorine atom [26], and leflunomide (LEF), an immunosuppressive disease-modifying antirheumatic drug (DMARD) containing three fluorine atoms,[27] were selected as drug models. Structural organization and morphology of these NPs were elucidated by DLS, solid-state NMR, and TEM analysis. In order to evaluate the eventual cytotoxicity of F-PLGA NPs *in vitro* tests on kidney glomerular cells were also performed. Finally, podocyte repair due to controlled delivery of DEX from F_9-PLGA NPs was demonstrated.

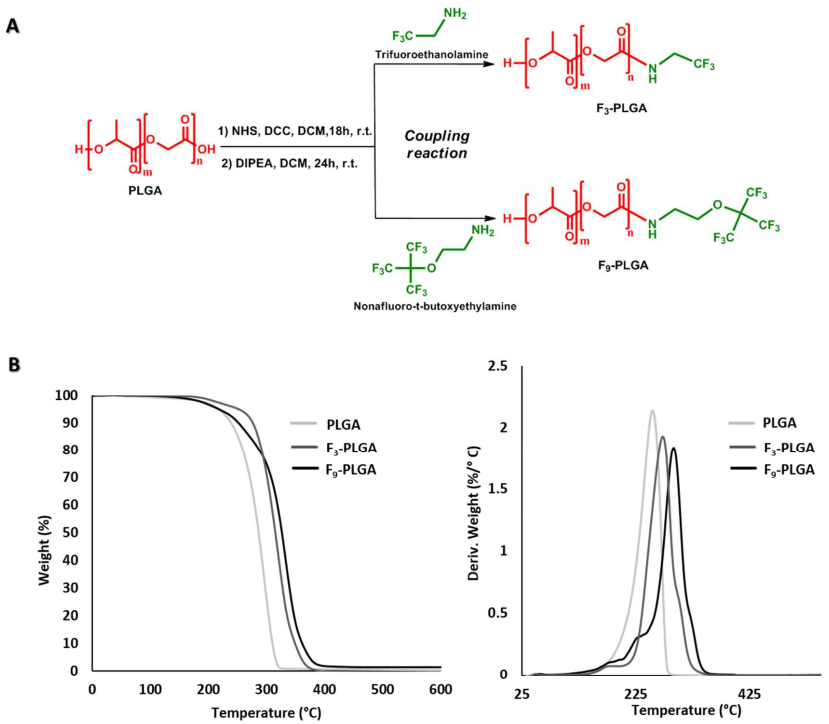

C

	T_{onset} (° C)	T_{endset} (° C)	$T_{deg.max.}$	Gl. Tr.
PLGA	89	280	254	30-42
F_3-PLGA	94	328	272	41-45
F_9-PLGA	93	345	292	38-47

Figure 1. Synthesis and chemical structures of the fluorinated PLGA (F-PLGA) derivatives: F_3-PLGA and F_9-PLGA respectively (**A**). TG curves (on the left) and second derivatives (on the right) of PLGA (light grey), F_3-PLGA (grey) and F_9-PLGA (black), by heating rate 10 °C min^{-1} starting from r.t. up to 550° (**B**). T_{onset}, T_{endset}, $T_{deg.max.}$ evaluated by TGA analysis and Glass Transition (Gl. Tr) estimated by DSC analysis relative to PLGA, F_3-PLGA and F_9-PLGA (**C**).

Materials and Methods

Materials

N–Hydroxysuccinimide ($C_4H_5NO_3$), N,N'-Dicyclohexylcarbodiimide ($C_{13}H_{22}N_2$), N,N-diisopropylethylamine ($[(CH_3)_2CH]_2NC_2H_5$), Acryloyl chloride (C_3H_3OCl), Triethylamine

($C_6H_{15}N$), Tris(2-carboxyethyl)phosphine hydrochloride ($C_9H_{15}O_6P \cdot HCl$), Methyl Iodide (CH_3I), Sodium Hydride (NaH) and Dexamethasone ($C_{22}H_{29}FO_5$) were purchased by Sigma Aldrich. 2,2,2- Trifluoroethanolamine ($C_2H_4NF_3$), Nonafluoro-t-butoxyethylamine HCl ($C_6H_7ClF_9NO$) and 3,3,3- Trifluoropropylmercaptan ($C_3H_5F_3S$) were purchased by FluoroChem. Leflunomide ($C_{12}H_9F_3N_2O_2$) was purchased by TCI Europe N.V. PLGA (LA:GA= 50:50, Mn≈ 8792) was provided by Solvay.

Synthesis of fluorinated PLGA

- **Synthesis of PLGA-NHS**

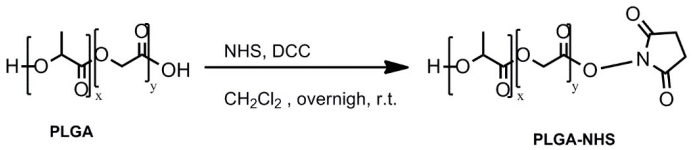

Scheme 1. Synthesis of PLGA-NHS.

PLGA was purified by precipitation in cold Et_2O. The purified PLGA (0.33 mmol, 1 eq) was dissolved in 10 mL of anhydrous CH_2Cl_2, then N-Hydroxysuccinimide (NHS) (1.32 mmol, 4 eq) was added. Subsequently, N,N'-Dicyclohexylcarbodiimide (DCC) (1.38 mmol, 4.2 eq) on ice bath was added and the solution became cloudy. The solution was left stirring at r.t. overnight. Then the urea-DCC solid, was removed by filtration and the PLGA-NHS was precipitated from the CH_2Cl_2 solution with cold Et_2O, and washed several times with the same solvent, obtaining a white solid PLGA-NHS.

^{1}H NMR (400 MHz, $CDCl_3$, δ): 5.30-5-19 (m, 1H, CH PLGA), 4.89-4.67 (m, 2H, CH_2 PLGA), 2.84 (m, 2H, CH_2), 1.58-1.59 (d, 3H, CH_3 PLGA).

- **Synthesis of ((2,2,2-trifluoroethyl)amide-terminated poly(-lactide–co–glycolide) (F_3-PLGA)**

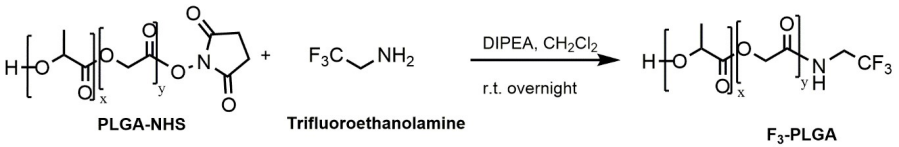

Scheme 2. Synthesis of ((2,2,2-trifluoroethyl)amide-terminated poly(-lactide–co–glycolide), (F_3-PLGA).

PLGA-NHS (0.33 mmol, 1 eq) was dissolved in 6 mL of anhydrous CH_2Cl_2, then 2,2,2-trifluoroethanolamine (1.27 mmol, 3.86 eq) and N,N-diisopropylethylamine (DIPEA) (1.43 mmol, 4.34 eq), with a slight modification with respect to the procedure reported in the literature [28], were added. The solution was left stirring overnight at r.t. under N_2 atmosphere. Then, the solution was concentrated and F_3-PLGA was precipitated with cold Et_2O. In order to increase the purity of the product, it was washed with Mq Water and dried under vacuum at 50° C. Finally, 238 mg of F_3-PLGA white electrostatic powder were obtained (10% yield, Mw 7312.24).

^{1}H NMR (400 MHz, $CDCl_3$, δ): 6.86-6.55 (brs, OH), 5.26-5-18 (m, 1H, CH PLGA), 4.89-4.67 (m, 2H CH_2 PLGA), 3.95 (m, 2H, CH_2), 1.58-1.59 (d, 3H, CH_3 PLGA).

^{13}C NMR (400 MHz, $CDCl_3$, δ): 169.49, 166.43, 69.25, 60.88, 40.30, 16.66.

^{19}F NMR (400 MHz, $CDCl_3$, δ): -72.49 (s, 3F, CF_3).

- **Synthesis of ((2-((1,1,1,3,3,3-hexafluoro-2(trifluoromethyl)propan-2-yl)oxy)ethyl)amide-terminated poly(-lactide–co–glycolide), (F_9-PLGA)**

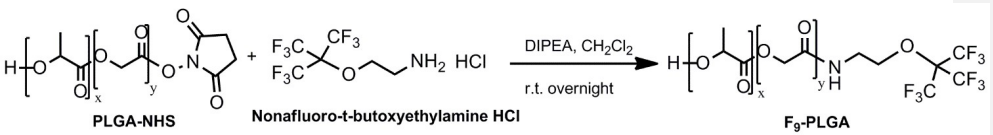

Scheme 3. Synthesis of ((2-((1,1,1,3,3,3-hexafluoro-2(trifluoromethyl)propan-2-yl)oxy)ethyl)amide-terminated poly(-lactide–co–glycolide), (F_9-PLGA).

PLGA-NHS (0.33 mmol, 1 eq) was dissolved in 6 mL of anhydrous CH_2Cl_2, then nonafluoro-t butoxyethylamine HCl (0.28 mmol, 1 eq) and N,N-diisopropylethylamine (DIPEA) (1.15 mmol, 4 eq) were added [28]. The solution was left stirring overnight at r.t. under N_2 atmosphere. Subsequently, the solution was concentrated and F_9-PLGA was precipitated with cold Et_2O. In order to increase the purity of the product, F_9-PLGA was washed with Brine solution and dried under vacuum at 50° C. 888 mg of white electrostatic powder were obtained (28% yield, Mw 9575.37).

^{1}H NMR (400 MHz, CDCl3, δ): 6.61 (brs, OH), 5.26-5.19 (m, 1H, CH PLGA), 4.88-4.60 (m, 2H, CH_2 PLGA), 4.12 (m, 2H, CH_2), 3.59 (m, 2H, CH_2), 1.57-1.59 (d, 3H, CH_3).

^{13}C NMR (400 MHz, CDCl3, δ): 169.52, 166.46, 69.29, 68.54, 60.90, 38.99, 16.69.

^{19}F NMR (400 MHz, CDCl3, δ) :-70.37 (s, 9F, CF_3).

Preparation of PLGA NPs. NPs were formulated by a solvent evaporation method in surfactant free conditions using at 1:1 acetone-water volume ratio with a final pH=6.4 (**Figure 2**). The procedure consists in the dropwise addition of PLGA or F-PGLA 10 mg/mL solution in acetone to a 1 mL of Mq Water. The obtained emulsion was left stirring for 15 min and the organic solvent was fully removed under vacuum and checked by ^{1}H NMR using deuterated acetone. Moreover,

F_9-PLGA NPs were formulated in phosphate buffer solution (PB) at different pH values from 6.4 to 8.0, keeping constant the volume ratio.

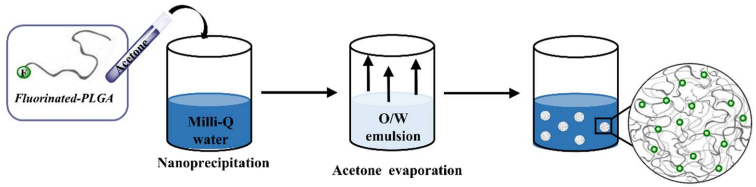

Figure 2. Schematic representation of solvent evaporation method for the formulation of F-PLGA NPs.

NP Drug Loading. The drug (dexamethasone/leflunomide) was solubilized in acetone to obtain a concentration of 1 mg/mL. Then 10 mg of polymer (PLGA/ F_9-PLGA) were solubilized in 1 ml of drug solution. Thus, this mix was dropwise added to 1 mL of Mq Water and the suspension was stirred at r.t. for 15min. Afterwards, the acetone was removed under vacuum and the NPs were lyophilized [29]. The lyophilized polymer was dissolved in 1 mL of acetonitrile. Then, it was 1:10 diluted in acetonitrile.

Dexamethasone (DEX) and Leflunomide (LEF) content was determined by HPLC analysis. Each sample was injected (10 µL) in a C18 reversed-phase chromatography column at 30 °C with a flow rate of 1 mL/min in a solution of acetonitrile-water 1:1. The DEX peak was detected after ~3 min and LEF peak after ~10 min. The detection wavelength was set at 254 nm. Calibration curves were previously obtained with different DEX and LEF concentrations (1, 0.5, 0.1, 0.01, 0,001 mg/mL). The Drug Loading (DL%) and Encapsulation Efficiency (EE%) values associated to each polymers were calculated according to the following equations[30,31]:

$$DL\% = 100 * \frac{Weight\ of\ Drug\ Encapsulated}{Weight\ of\ Drug\ Encapsulated + Weight\ of\ Polymer\ Nanoparticles}$$

$$EE\% = 100 * \frac{Weight\ of\ Drug\ Encapsulated\ In\ Polymer\ Nanoparticles}{Weight\ of\ Drug\ Used\ in\ Encapsulation\ Method}$$

LDH Cytotoxicity. NPs cytotoxicity was measured using LDH-Cytotoxicity Colorimetric Assay Kit (BioVision Incorporated). Briefly 8000 per well of conditionally immortalized human podocytes (HCiPodo) or conditionally immortalized human glomerular endothelial cells (HCiGEnC) (both from University of Bristol, Bristol, UK) were plated on a 96-well plate and cultured at 37°C respectively in RPMI-1640 with 10% FCS, 5 µg/mL transferrin, 5 ng/mL sodium selenite, 0.12 U/mL insulin, 100 U/mL penicillin, 100 mg/mL streptomycin or with EGM2-MV medium containing foetal calf serum (5%) and growth factors as supplied (Lonza, Walkersville, MD, USA) for 3-4 days. Then, the culture medium was replaced by medium containing different concentration of NPs (0.01-2mg/mL) which was incubated with cells for 24 hours. For positive control (high control), 10 µL of cell Lysis solution was added and incubated for 24 hours, while the low control was referred to cells incubated only with standard medium. At the end of incubation, the plate was gently shacked for some minutes and centrifuged at 600 x g for 10 min. 10 µL of culture medium from each well was transferred into a new optically clear 96-well plate, and 100 ul of LDH Reaction Mix was added to each well and incubated at room temperature for 30 min. The absorbance of all controls and samples was measured with 450 nm filter using SAFAS Spectrophotometry (Monaco). The cytotoxicity was calculated using the equation: Normalised Cytotoxicity = (Test sample-Low control)/(High control-Low control) ; Low control : normal cells; High control : cells treated with lysis buffer.

Commentato [RG1]: FCS spiegare l'acronimo: foetal calf serum?

Fluorescence Microscopy Examination. HciPodo and HCiGEnC were cultured on coverslips and fixed with 4% of paraformaldehyde at room temperature for 10 min. After washing, cells were permeabilized with 0.3% of Triton in PBS for 5 min and incubated with 1% of bovine serum albumin in PBS at room temperature for 30 min.

Phalloidin-FITC (Sigma-Aldrich) at 1:100 dilution together with DAPI at 1:1000 dilution (Sigma-Aldrich) was added, and the cells were incubated for 1 h. After 3 times washing with PBS, the cells were mounted with Fluorsave aqueous mounting medium (Merck, Milano, Italy). Images were acquired using a Zeiss AxioObserver microscope equipped with a high resolution digital videocamera (AxioCam, Zeiss) and an Apotome system for structured illumination, and recorded by the AxioVision software, version 4.8.

DEX Release on Podocytes. HciPodo were plated on a 35 mm Petri dish containing four cell culture coverslips and cultured at 37 °C for 3−4 days. Afterwards, cells were incubated with 0.8 μM Adriamycin (ADR, Sigma-Aldrich) in cell culture medium for 24 h. After 24h incubation, ADR was replaced by fresh medium (as the control group) or medium with a different concentration of NPs loaded with Dexamethasone (100 μM or 10 μM) and incubated for another 24 or 48 h. Cells were finally washed thrice with PBS and characterized by fluorescence microscopy as described above.

Methods

Attenuated total reflectance FTIR (ATR-FTIR) spectra were obtained with a Thermo Scientific Nicolet iS50 FTIR spectrometer, equipped with an iS50 ATR accessory (Thermo Scientific, Madison, USA). NP dispersions were deposited by drop casting on the ATR probe and the solvent was left evaporating before the measurement.

^{1}H, ^{13}C, and ^{19}F Nuclear Magnetic Resonance (NMR) spectra were performed at r. t. on a Bruker AV400 spectrometer. Chemical shifts are reported in parts per million (ppm). Multiplicities are reported as follows: s (singlet), brs (broad singlet), d (doublet), m (multiplet). Trifluoroacetic acid (TFA) was added as external standard, with chemical shift set at ~ -75.45 ppm, for the ^{19}F NMR

spectra of the F_9-PLGA_NPs dispersions, formulated at different water:acetone ratio and at different pH values.

^{19}F T_1 and T_2 measurements were recorded at 305 K on a Bruker AV400 spectrometer operating at 400 MHz for the ^1H nucleus. The inversion recovery and the CPMG pulse sequences were used for the measures of T_1 and T_2, respectively.

Solid-state NMR measurements were performed on a Bruker Avance II 400 instrument operating at 400.2, 100.6 and 376.5 MHz for ^1H, ^{13}C and ^{19}F nuclei, respectively. For ^1H-^{13}C and ^{19}F-^{13}C CPMAS spectra, the powder samples were packed in 4 mm diameter cylindric zirconia rotors (volume of 80 µL) and spun at 12 kHz. A ramp cross-polarization sequence was used with a contact time of 3.0 ms, a 90° pulse of 2.1 (^1H) and 4.0 (^{19}F) µs and optimized recycle times in the range 1-2 (^1H) and 1-40 (^{19}F) s, depending on the sample, and 6600-25000 scans. In all spectra, the two pulse phase modulation (TPPM) decoupling scheme with a 119.0 kHz radiofrequency field (^1H) or a Swept-frequency two-pulse phase modulation (SWf-TPPM) (^{19}F) with a 83 kHz radiofrequency field was used.

^{19}F MAS and ^{19}F DQ MAS spectra were acquired in 2.5 mm diameter cylindric zirconia rotors (volume of 12 µL) with a spinning speed of 32 kHz. ^{19}F MAS spectra were acquired with a depth sequence ($\pi/2$-π-π) for the suppression of the probe background signal (^{19}F 90° =5.2 µs; scans = 16; relaxation delay = 5.3 s for LEF@F_9-NPs and 2.4 s for F_9-NPs).

The 2D ^{19}F DQ MAS experiments were performed with the back-to-back (BABA) recoupling pulse sequence with excitation time durations of one rotor period (^{19}F 90° =5.2 µs; 64 scans; 128 t1 increments). The ^{13}C and ^{19}F chemical shift scales were calibrated through the methylenic glycine signal (^{13}C peak at 43.7 ppm) andteflon (^{19}F signal at -122 ppm) as external standards.

Gel Permeation Chromatography (GPC) measurements were carried out with a Jasco instrument equipped with: 2055i auto sampler; RI-2031 refractive index detector; CO-2060 plus oven column; PU-2080 pump; three PLgel 300 mm·7.5 mm (5 μm particle size) (10E4, 10E5, 500 A) and a PLgel 50 mm·7.5 mm (5 μm particle size) guard. Calibration is done using a polystyrene calibration kit (by RESTEK and Sigma-Fluka). The samples were dissolved in THF at the concentration of 10 mg/mL and injected (50 μL) in the chromatography column at 35 °C with a THF flow rate of 0.5 mL/min.

Thermogravimetric analysis (TGA) of the samples, weighed in aluminum pans, was performed using a thermogravimetric analyzer TGA Q500/QNX/PlatinumTM. The TG curves of PLGA, F_3-PLGA and F_9-PLGA were obtained by heating with a rate of 10 °C/min from r. t. up to 550° C. T_{onset} and T_{endset} values (the temperatures at which the mass loss begins and ends, respectively) were evaluated by TG curves. Moreover, $T_{deg.max.}$ (temperature of the maximum mass loss) were obtained by the derivative of the TG curves (Dr. TG).

Differential scanning calorimetry (DSC) measurements were performed by a Mettler Toledo DSC823 using 40 μL aluminum pans and Mettler STARe software for calculations. The DSC curves of PLGA, F_3-PLGA and F_9-PLGA were obtained by heating with a rate of 10 °C/min, starting from 20° C up to 350° C.

Transmission Electron Microscopy (TEM) images were acquired by using a Delong America LVEM5 microscope, equipped with a field emission gun and operating at 5 kV. Samples were prepared by dropping NP dispersions (0.3 mg/mL and 3 mg/mL) on carbon-coated copper grids and letting them dry overnight. TEM image analysis was performed using ImageJ software.

Statistical analysis was based on the measurement of about 1000-4000 NPs. Size distributions were fitted by a Lorentz equation using IgorPro 4.02.

Dynamic Light Scattering (DLS) measurements were performed on an ALV apparatus equipped with ALV- 5000/EPP Correlator, special optical fiber detector and ALV/CGS-3 Compact goniometer. The light source is He-Ne laser (λ = 633 nm), 22 mW output power. Measurements were performed at 25 °C. Approximately 1 mL of sample solution was transferred into the cylindrical Hellma scattering cell. Data analysis has been performed according to standard procedures and auto-correlation functions were analyzed through a constrained regularization method (Laplace inversion of the time auto-correlation functions), CONTIN, for obtaining the particle size distribution.

High Performance Liquid Chromatography (HPLC) measurements were performed on a JASCO® HPLC equipped with: 2057 autosampler; RI-2031 refraction index detector; UV-Vis detector, CO-2060 plus oven column; PU-2080 pump; MD-2018 photodiode array PDA detector; C18 column (5 µm particle size) 150 mm·4.6 mm (length × diameter), mobile phase consisted of 50/50 (v/v) water/acetonitrile. Evaluation of the drug concentration was done using the UV-Vis detector. The DEX peak was detected after ~3 min and LEF peak after ~10 min. The detection wavelength was set at 254 nm. Calibration curves were previously obtained with different DEX and LEF concentrations (1, 0.5, 0.1, 0.01, 0,001 mg/mL).

Results and Discussion

PLGA functionalization. PLGA was functionalized with two different fluorinated molecules *via* amide-coupling reaction with a slight modification with respect to the procedure reported in literature [28]. After PLGA activation by NHS, the PLGA-NHS intermediate was obtained and

covalently conjugated to either Trifluoroethanolamine or Nonafluoro-t-butoxyethylamine HCl, by using DIPEA, with the production of two new fluorinated polymers, F_3-PLGA and F_9-PLGA (**Figure 1A**), containing three and nine magnetically equivalent ^{19}F atoms respectively (see "Materials and Methods" section for the detailed synthetic procedure). Molecular number (Mn), Molecular weight (Mw) and Dispersity (Đ) relative to PLGA, F_3-PLGA and F_9-PLGA were evaluated by GPC analysis (**Table S1**). Moreover, the thermal stability of PLGA, F_3-PLGA and F_9-PLGA was estimated by TGA and DSC analysis. TG curves of all the samples were characterized by only one mass loss stage with an increase of the thermal stability upon fluorination and a starting degradation point at around 200° C (**Figure 1B**). DSC curves showed a glass transition (Gl. Tr.) phase between 30°- 47° C (**Figure 1C**) and no melting point for all the samples, indicating their amorphous nature in agreement with the literature [32].

Preparation and Characterization of F-PLGA NPs. PLGA (PLGA_NPs), F_3-PLGA (F_3-PLGA_NPs) and F_9-PLGA (F_9-PLGA_NPs) NPs were formulated by a solvent evaporation method in surfactant free conditions (see **Figure 2** and the "Material and Methods" section for the formulation details) using a 1:1 acetone-water volume ratio with a final pH=6.4.

The obtained NPs were characterized by DLS, TEM and solution ^{19}F NMR techniques. DLS analysis of PLGA_NPs , F_3-PLGA_NP and F_9-PLGA_NP dispersions showed that they were characterized by an averaged hydrodynamic radii (R_H) of 61 ± 5 nm (**Table S2**); 54 ± 6 nm (**Figure 3B**, **Table S2**) and 58 ± 6 nm (**Figure 4B**, **Table S2**), respectively and a good polydispersity (PDI) (**Table S2**). The intensity-weighted $<R_H>$ size distribution evaluated by CONTIN analysis was in agreement with the TEM size distribution for both samples (**Figures 3A** and **4A**). More importantly, a characteristic ^{19}F-NMR signal at around, -72 ppm and -70 ppm were recognized for

F_3-PLGA_NPs (**Figure 3C**) and F_9-PLGA_NPs (**Figure 4C**), respectively indicating that self-assembly did not impair the mobility of the fluorinated chains.

Moreover, in order to evaluate the efficiency of F_3-PLGA NPs and F_9-PLGA NPs as ^{19}F-NMR probe, their T_1 and T_2 relaxation times were evaluated at physiological pH. F_3-PLGA_NPs and F_9-PLGA_NPs showed T_1 values of 537 ms and 625 ms and T_2 values of 122 ms and 60 ms, respectively, in agreement with values found for ^{19}F MRI active NP systems [33], indicating their suitability for ^{19}F MRI applications. As expected, the increase of ^{19}F atoms in the molecular structure significantly affected the intensity ^{19}F NMR signal of F_9-PLGA_NPs with respect to that of F_3-PLGA_NPs at the same polymer concentration. Therefore, further characterizations were focused on the most promising F_9-PLGA_NPs.

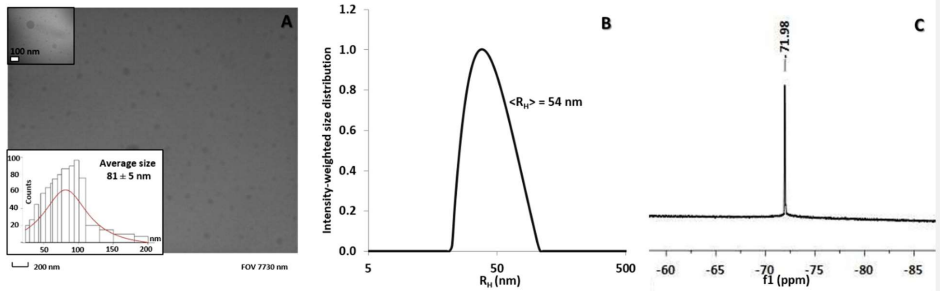

Figure 3. TEM image (**A**), of a dispersion of F_3-PLGA_NPs formulated at 1:1 acetone-water volume ratio. The distribution size was confirmed by DLS analysis (**B**). ^{19}F NMR spectrum (**C**) shows the characteristic ^{19}F signal of F_3-PLGA_NPs.

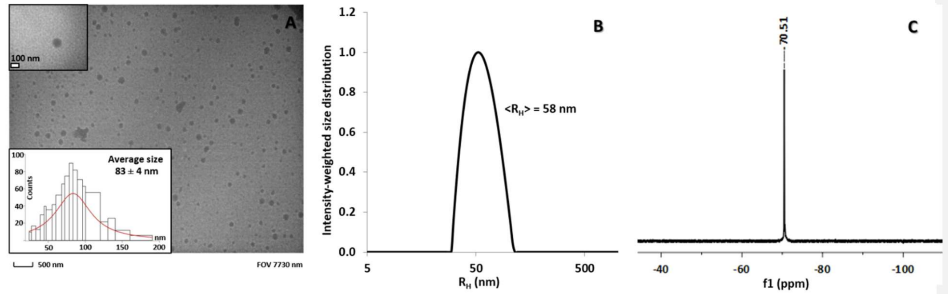

Figure 4. TEM image (**A**), of a dispersion of F_9-PLGA_NPs formulated at 1:1 acetone-water volume ratio. The distribution size was confirmed by DLS analysis (**B**). The ^{19}F-NMR spectrum (**C**) shows the characteristic ^{19}F signal of fluorinated F_9-PLGA_NPs.

It is known that several parameters such as type of solvent, polymer concentration, solvent ratios etc. can generally influence the features of PLGA NPs prepared by solvent evaporation method [34]. In order to investigate these aspects, F_9-PLGA_NPs were formulated at the same polymer concentration (10 mg/ml) and acetone-water ratio (1:1), but at different pH values (ranging from 6.4 to 8.0). The integral values extracted for the ^{19}F NMR signals of the F_9-PLGA_NP formulations linearly increased with pH passing from 6.4 to 8.0 (**Figure S1**) without significantly shifting with respect to TFA used as internal reference. Moreover, DLS data showed comparable results in terms of colloidal stability and hydrodynamic size distributions (**Table S3**). Regarding these preliminary studies, we suppose that the linear response to ^{19}F NMR is probably related to intramolecular interactions among the different moieties of the polymer, which could affect the mobility of the fluorinated chains, during the self-assembly process. This is only a preliminary study and a more in-depth analysis must be done in order to better understand this phenomenon.

F-PLGA NPs as multifunctional tools. The efficiency of F_9-PLGA NPs to function as ^{19}F NMR detectable drug carriers was proven by testing their ability to encapsulate hydrophobic drugs and also by evaluating the ^{19}F T_1 and T_2 relaxation times on both F_9-PLGA NPs and drug loaded F_9-PLGA NPs. The capacity of encapsulating hydrophobic drugs for PLGA and F_9-PLGA NPs was proven using dexamethasone, DEX, (**Figure 5A**), and leflunomide, LEF (**Figure 5B**). The

hydrophobic nature of these drugs is demonstrated by their logP values: ≈1.68 (polar surface area, PSA, 94.83 Å2) for DEX and ≈2.52, (PSA 55.10 Å2) for LEF.

Drug loaded PLGA and F_9-PLGA NPs were formulated using the same acetone-water emulsion method [29], with addition of the drug in the organic solution. The drug loading capacity % (DL%) and encapsulation efficiency % (EE%) of F_9-PLGA_NPs were evaluated and compared to that of PLGA NPs in the same conditions. The process was optimized by keeping constant the polymer: drug ratio, and by increasing the concentration of both components at two different polymer: drug weight ratios 10:1 (DEX@F_9-PLGA/PLGA_1 and LEF@F_9-PLGA/PLGA_1) and 20:2 (DEX@F_9-PLGA/PLGA_2 and LEF@F_9-PLGA/PLGA_2).

First, DEX and LEF loading was qualitatively evaluated by ATR-FTIR analysis by detecting the characteristic signal of the drugs (**Figures S2** and **S3**).

A

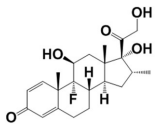

Dexamethasone

	DEX@PLGA_1	DEX@F_9PLGA_1	DEX@PLGA_2	DEX@F_9PLGA_2
<R_H> (nm)	59±5	53±5	66±7	65±6
PDI	0.15	0.15	0.23	0.16
DL (%)	2.1	4.2	1.6	3.0
EE (%)	16.5	29.0	12.5	18.5

B

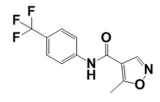

Leflunomide

	LEF@PLGA_1	LEF@F_9PLGA_1	LEF@PLGA_2	LEF@F_9PLGA_2
<R_H> (nm)	86±7	60±6	74±5	63±6
PDI	0.23	0.14	0.51	0.16
DL (%)	2.1	2.0	5.2	7.6
EE (%)	16.0	18.5	48.0	69.0

Figure 5. DEXchemical structure (**A**) and LEF chemical structure (**B**). In Tables are reported the DLS, DL and LL data relative to DEX@F_9-PLGA and to LEF@F_9-PLGA NPs formulated both at 1:10 and 2:20 drug: polymer ratio.

More importantly, the ^{19}F signal of F_9-PLGA (at around -72 ppm), in both ^{19}F NMR spectra of DEX@F_9-PLGA_2 and LEF@F_9-PLGA_2 has been detected (**Figure S4**). Moreover, in the ^{19}F NMR spectrum of LEF@F_9-PLGA_2 is also recognized the ^{19}F signal of LEF at around -62 ppm (**Figure S4B**). Unfortunately, a decrease of T_2 value for both DEX@F_9-PLGA_NPs and LEF@F_9-PLGA_NPs with respect to the starting F_9-PLGA_NPs (**Table S4**) was observed indicating that

the drug loading process partially impairs the mobility of the fluorinated chains. Then, the morphology was investigated by DLS and TEM analysis: average sizes of 83 ± 5 nm (DEX@F_9PLGA) and 91 ± 5 nm (LEF@F_9PLGA) were estimated by TEM (**Figure S5**) in good agreement with DLS results (**Figure 5**). Both loaded NPs showed a higher value of $<R_H>$ with respect to that of the corresponding unloaded NPs (**Table S2**). Generally, LEF/DEX@F_9-PLGA_NPs showed higher homogeneity, lower PDI values (**Figure 5**) and higher stability in a wider range of concentrations with respect to the corresponding drug loaded PLGA NPs (**Figure 5**). The quantitative amount of DEX and LEF entrapped within the NPs was instead determined by HPLC analysis (see "Materials and Methods" section for the experimental details).

Considering both encapsulation efficiency (EE%) and drug loading capacity (DL%) results two observations can be made: at both polymer/drug weight ratios F_9-PLGA was able to encapsulate a higher amount of DEX/LEF with respect to the unmodified PLGA and both F_9-PLGA and PLGA showed higher values of EE% and DL% for LEF with respect to those obtained for DEX at the optimal polymer/drug ratio. Thus, a combination of two different effects govern the drug encapsulation process: first, considering that PLGA is commonly used to entrap drugs characterized by a high hydrophobicity, it is reasonable that both F_9-PLGA and PLGA NPs entrapped a higher amount of the more hydrophobic LEF than DEX. While general higher encapsulation yields observed for F_9-PLGA NPs with respect to the unmodified PLGA NPs might be due to F-F interactions among the fluorinated groups of the polymer and the drugs [35].

This latter aspect was investigated through solid-state NMR of the lyophilized LEF@F_9-PLGA formulations. In **Figures S6** and **S7** are reported the ^{1}H-^{13}C and ^{19}F-^{13}C CPMAS NMR spectra of LEF@F_9-PLGA together with F_9-PLGA formulation and pure LEF. The ^{1}H-^{13}C CPMAS NMR spectrum of LEF@F_9-PLGA, shows the presence of the drug in the lyophilized NPs according to

its weight percentage (about 7%). This agrees with the ^{19}F MAS SSNMR spectrum (**Figure S8** in comparison with those of pure LEF and F_9-PLGA) which is characterized by two different resonances (-60.7 and -59.5 ppm) for the LEF molecule loaded into the NPs. The two signals indicate the presence of two different environments for LEF inside the NPs, in agreement with the broad ^{13}C resonance observed in the ^{19}F-^{13}C CPMAS spectrum (**Figure S7**). Moreover, 2D ^{19}F DQ MAS experiments were performed to highlight correlations due to pairs of through-space dipolar coupled fluorine atoms, i.e. to close in space fluorine atoms. In particular, they are able to probe LEF-LEF or/and LEF@F_9-PLGA NPs CF_3 interactions, thus providing insights on the LEF distribution inside the nanoparticles. The 2D spectra of F_9-PLGA NPs and LEF@F_9-PLGA NPs are reported in **Figure S9**. The spectrum of F_9-PLGA NPs shows an autocorrelation (δ_{DQ}=-70-70 = -140 ppm) indicating that the NP self-assembly brings the F_9 group close to each other. On the other hand, the 2D ^{19}F DQ MAS of LEF@F_9-PLGA NPs is characterized by autocorrelations only for the LEF resonances (δ_{DQ}=-60.7-60.7 =-121.4 and δ_{DQ}=-59.5-59.5 = -119.0). This suggests that the LEF molecules within the NPs are close in space, with the $–CF_3$ groups pointing one towards each other, whereas no interactions with the $–CF_3$ groups of the NPs are present. Thus, we can conclude that the drug encapsulation process is driven by a hydrophobic effect. Due to its higher hydrophobicity F_9-PLGA is much able to entrap a higher amount of hydrophobic drugs respect to the not fluorinated PLGA. In addition, DEX is less hydrophobic than LEF, therefore it is reasonable than a higher EE% was estimated.

PLGA NPs loaded with DEX were assessed in terms of cytotoxicity in vitro on immortalized human glomerular endothelial cells (HCiGEnC) and podocytes (HCiPodo), taking into account the constant interaction of the NPs during in vivo blood circulation with the cells of the kidney glomerular filtration barrier [36,37]. Cells were cultured at 37 °C in presence of different

concentration of nanoparticles (0.01–2 mg/mL) for 24 h. Lactate Dehydrogenase (LDH) colorimetric assay was selected for the test as it was proven to be an efficient indicator of cytotoxicity for kidney glomerular cells [37,38]. PLGA and F_9-PLGA, with and without loaded dexamethasone, showed negligible cytotoxicity up to a concentration of 1 mg/mL (**Figure 6**), which confirmed the high biocompatibility of these polymeric nanomaterials even when fluorinated and drug-loaded. The therapeutic effect of DEX-loaded F_9-PLGA NPs was also assessed on damaged podocytes *in vitro*. Alteration of their cytoskeleton morphology is known to be a good indicator of pathological condition in chronic kidney diseases [37,39], therefore the efficacy of DEX@F_9PLGA NPs on these cells was assessed by evaluating F-actin orientation on HCiPodo cells before and after the treatment [37,38]. Cell damage was induced with Adriamycin (ADR) incubation for 24 h, as confirmed by the reduced density and irregular distribution of the actin fibres (green-phalloidin staining), together with a disappearance of cell protrusions (**Figure 6A1**). After 48 h incubation with the NPs, podocytes displayed a more regular distribution of F-actin along the whole cell body and processes, which indicated a recovered healthy morphology (**Figure 6B1**). These results demonstrated that DEX bioactivity was retained during the particle manufacturing process.

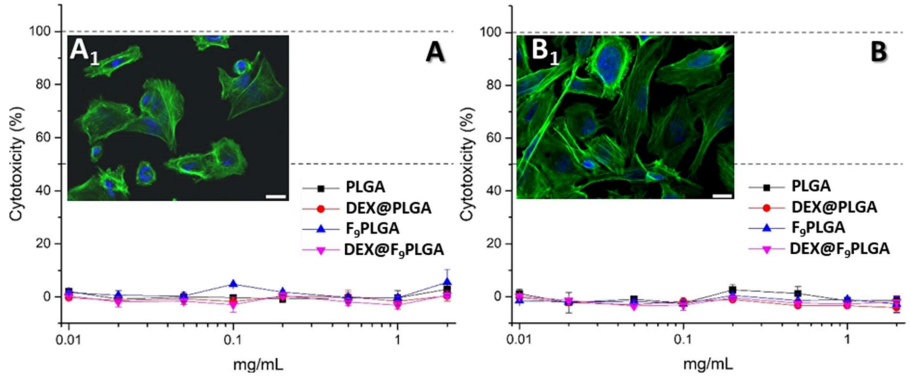

Figure 6. LDH assay on HCiGEnC (**A**) and HCiPodo cells (**B**) incubated with NPs (PLGA, DEX@PLGA, F_9PLGA, DEX@F_9PLGA) for 24 h, at concentration from 0.01 to 2 mg/mL. Y-axis: Normalised Cytotoxicity = (Test sample-Low control) / (High control-Low control); Low control: normal cells; High control: cells treated with lysis buffer A. DEX release from DEX@F_9PLGA NPs in water at 37 °C (error bars indicate± SD from experiments run in triplicate). HCiPodo cells (stained by green phalloidin and DAPI, scale bar 20 μm) damaged by ADR (**B1**) and incubated for 48 h with DEX@F_9PLGA (DEX concentration 10μM).

Conclusions

Overall, synthesis, characterization and formulation of two new F-PLGA co-polymers, F_3-PLGA and F_9-PLGA, was reported. F_9-PLGA NPs were found more promising in terms of intensity of the ^{19}F-NMR signal. The relaxivity properties of the assembled NPs considering the T_1 and a T_2 values obtained are promising for using these dispersions in ^{19}F-MRI. In addition, the F_9-PLGA NPs are able to encapsulate hydrophobic drugs more efficiently than unmodified PLGA NPs.

Thus, we believe that these formulations are optimal candidates as multimodal drug delivery systems, which can be in vivo tracked by ^{19}F-MRI.

ASSOCIATED CONTENT

Supporting Information.

- Molecular number (Mn), Molecular weight (Mw) and Dispersity (Đ) of PLGA, purified PLGA, F_3-PLGA and F_9-PLGA, respectively. The data are obtained by GPC analysis (**Table S1**).

- DLS data of PLGA, F_3-PLGA and F_9- PLGA NPs formulated at pH 6.4 and at NP concentration 10mg/mL (**Table S2**).

- ^{19}F-NMR spectra of F_9-PLGA_NPs formulated at different pH values (ranging from 6.4 to 8.0) and compared to a trifluoroethanol standard solution (TFA). Linear fit of the integrals of the peak normalized for the peak of the TFA is reported. (**Figure S1**).

- DLS data of F_9- PLGA NPs formulated at different pH values (ranging from 6.4 to 8.0) and at the same NP concentration 10mg/mL (**Table S3**).

- Qualitatively evaluation of the DEX encapsulation degree in F_9-PLGA_NPs by ATR-FTIR analysis. DEX@F_9-PLGA_2 showed the characteristic vibration modes both of DEX and F_9-PLGA_NPs (**Figure S2**).

- Detection of characteristic vibration modes of LEF and F_9-PLGA_NPs in ATR-FTIR spectrum of LEF@F_9-PLGA_2 in order to qualitatively evaluated the encapsulation degree of LEF in F_9-PLGA_NPs (**Figure S3**).

- The ^{19}F NMR spectra of DEX@F_9PLGA_2 (A) and LEF@F_9PLGA_2 (B) (**Figure S4**).
- T_1 and T_2 values of F_3PLGA_NPs, F_9PLGA_NPs, DEX@F_9PLGA_2 and LEF@F_9PLGA_2 dispersions evaluated at physiological pH (**Table S4**).

- TEM images of DEX@F_9-PLGA and LEF@F_9-PLGA formulations and distribution sizes. (**Figure S5**).

- ^{1}H-^{13}C (100.6 MHz) CPMAS SSNMR spectra of F_9-PLGA NPs, LEF and LEF@F_9-PLGA NPs, acquired at a spinning speed of 12 kHz (**Figure S6**).

- ^{19}F-^{13}C (100.6 MHz) CPMAS SSNMR spectra of F_9-PLGA, LEF and LEF@F_9-PLGA NPs, acquired at a spinning speed of 12 kHz (**Figure S7**).

- ^{19}F (376.5 MHz) MAS SSNMR spectra of F_9-PLGA and LEF@F_9-PLGA NPs, acquired at a spinning speed of 32 kHz (**Figure S8**).

- ^{19}F (376.5 MHz) DQ MAS spectrum of F_9-NPs (A) and LEF@F_9_NPs (B), acquired at a spinning speed of 32 kHz and using one period of BABA recoupling (**Figure S9**).

AUTHOR INFORMATION

Corresponding Author

*E-mail: francesca.baldelli@polimi.it

*E-mail: pierangelo.metrangolo@polimi.it

Author Contributions

The manuscript was written through contributions of all authors. All authors have given approval to the final version of the manuscript. ‡These authors contributed equally. (match statement to author names with a symbol)

Formattato: Inglese (India)
Codice campo modificato
Formattato: Inglese (India)
Formattato: Inglese (India)

Funding Sources

This research project was supported by Solvay Specialty Polymers.

Notes

Any additional relevant notes should be placed here.

ACKNOWLEDGMENT

We thank Solvay Specialty Polymers for supporting and funding this research project.

ABBREVIATIONS

NPs, nanopartcles; PLGA, poly(lactic-co-glycolic acid); F-PLGA, fluorinated co-polymers ; CAs, fluorinated contrast agents; PFC, perfluorinated molecules; PFPE, perfluoropolyethers; T2, transverse relaxation time; T1, longitudinal (or spin-lattice) relaxation time; NHS, N-Hydroxysuccinimide; DIPEA, N,N-Diisopropylethylamine; DEX, dexamethasone; LEF, lefluonomide; DL, Drug Loading; EE, Encapsulation Efficiency; HCiGEnC, Human glomerular endothelial cells; HCiPodo, podocytes; LDH, Lactate Dehydrogenase; ADR, Adriamycin.

REFERENCES

1. Chen, G.; Roy, I.; Yang, C.; Prasad, P.N. Nanochemistry and Nanomedicine for Nanoparticle-based Diagnostics and Therapy. *Chemical Reviews* **2016**, *116*, 2826-2885, doi:10.1021/acs.chemrev.5b00148.
2. Lal, S.; Perwez, A.; Rizvi, M.A.; Datta, M. Design and development of a biocompatible montmorillonite PLGA nanocomposites to evaluate in vitro oral delivery of insulin. *Applied Clay Science* **2017**, *147*, 69-79, doi:https://doi.org/10.1016/j.clay.2017.06.031.
3. Calderó, G.; Fornaguera, C.; Zadoina, L.; Dols-Perez, A.; Solans, C. Design of parenteral MNP-loaded PLGA nanoparticles by a low-energy emulsification approach as theragnostic platforms for intravenous or intratumoral administration. *Colloids and Surfaces B: Biointerfaces* **2017**, *160*, 535-542, doi:https://doi.org/10.1016/j.colsurfb.2017.09.060.
4. Baghaei, B.; Saeb, M.R.; Jafari, S.H.; Khonakdar, H.A.; Rezaee, B.; Goodarzi, V.; Mohammadi, Y. Modeling and closed-loop control of particle size and initial burst of PLGA biodegradable nanoparticles for targeted drug delivery. *Journal of Applied Polymer Science* **2017**, *134*, 45145, doi:10.1002/app.45145.

5. Sivakumar, B.; Aswathy, R.G.; Romero-Aburto, R.; Mitcham, T.; Mitchel, K.A.; Nagaoka, Y.; Bouchard, R.R.; Ajayan, P.M.; Maekawa, T.; Sakthikumar, D.N. Highly versatile SPION encapsulated PLGA nanoparticles as photothermal ablators of cancer cells and as multimodal imaging agents. *Biomaterials Science* **2017**, *5*, 432-443, doi:10.1039/C6BM00621C.
6. Xu, Y.; Kim, C.-S.; Saylor, D.M.; Koo, D. Polymer degradation and drug delivery in PLGA-based drug–polymer applications: A review of experiments and theories. *Journal of Biomedical Materials Research Part B: Applied Biomaterials* **2017**, *105*, 1692-1716, doi:10.1002/jbm.b.33648.
7. Lee, S.-J.; Kim, H.-J.; Huh, Y.-M.; Kim, I.W.; Jeong, J.H.; Kim, J.-C.; Kim, J.-D. Functionalized Magnetic PLGA Nanospheres for Targeting and Bioimaging of Breast Cancer. *Journal of Nanoscience and Nanotechnology* **2018**, *18*, 1542-1547, doi:10.1166/jnn.2018.14220.
8. Li, Y.; Wu, M.; Zhang, N.; Tang, C.; Jiang, P.; Liu, X.; Yan, F.; Zheng, H. Mechanisms of enhanced antiglioma efficacy of polysorbate 80-modified paclitaxel-loaded PLGA nanoparticles by focused ultrasound. *Journal of Cellular and Molecular Medicine* **2018**, *22*, 4171-4182, doi:10.1111/jcmm.13695.
9. Swy, E.R.; Schwartz-Duval, A.S.; Shuboni, D.D.; Latourette, M.T.; Mallet, C.L.; Parys, M.; Cormode, D.P.; Shapiro, E.M. Dual-modality, fluorescent, PLGA encapsulated bismuth nanoparticles for molecular and cellular fluorescence imaging and computed tomography. *Nanoscale* **2014**, *6*, 13104-13112, doi:10.1039/C4NR01405G.
10. Tirotta, I.; Dichiarante, V.; Pigliacelli, C.; Cavallo, G.; Terraneo, G.; Bombelli, F.B.; Metrangolo, P.; Resnati, G. 19F Magnetic Resonance Imaging (MRI): From Design of Materials to Clinical Applications. *Chemical Reviews* **2015**, *115*, 1106-1129, doi:10.1021/cr500286d.
11. Tirotta, I.; Mastropietro, A.; Cordiglieri, C.; Gazzera, L.; Baggi, F.; Baselli, G.; Bruzzone, M.G.; Zucca, I.; Cavallo, G.; Terraneo, G., et al. A Superfluorinated Molecular Probe for Highly Sensitive in Vivo19F-MRI. *Journal of the American Chemical Society* **2014**, *136*, 8524-8527, doi:10.1021/ja503270n.
12. Srinivas, M.; Boehm-Sturm, P.; Figdor, C.G.; de Vries, I.J.; Hoehn, M. Labeling cells for in vivo tracking using 19F MRI. *Biomaterials* **2012**, *33*, 8830-8840, doi:https://doi.org/10.1016/j.biomaterials.2012.08.048.
13. Preslar, A.T.; Tantakitti, F.; Park, K.; Zhang, S.; Stupp, S.I.; Meade, T.J. 19F Magnetic Resonance Imaging Signals from Peptide Amphiphile Nanostructures Are Strongly Affected by Their Shape. *ACS Nano* **2016**, *10*, 7376-7384, doi:10.1021/acsnano.6b00267.
14. Srinivas, M.; Heerschap, A.; Ahrens, E.T.; Figdor, C.G.; Vries, I.J.M.d. 19F MRI for quantitative in vivo cell tracking. *Trends in Biotechnology* **2010**, *28*, 363-370, doi:https://doi.org/10.1016/j.tibtech.2010.04.002.
15. Bo, S.; Yuan, Y.; Chen, Y.; Yang, Z.; Chen, S.; Zhou, X.; Jiang, Z.-X. In vivo drug tracking with 19F MRI at therapeutic dose. *Chemical Communications* **2018**, *54*, 3875-3878, doi:10.1039/C7CC09898G.
16. Anne H. Schmieder, S.D.C., Jochen Keupp,Samuel A. Wickline,Gregory M. Lanza. Recent Advances in ¹⁹Fluorine Magnetic Resonance Imaging with Perfluorocarbon Emulsions. *Engineering* **2015**, *1*, 475-489, doi:10.15302/j-eng-2015103.
17. Ahrens, E.T.; Flores, R.; Xu, H.; Morel, P.A. In vivo imaging platform for tracking immunotherapeutic cells. *Nature Biotechnology* **2005**, *23*, 983-987, doi:10.1038/nbt1121.

18. Amiri, H.; Srinivas, M.; Veltien, A.; van Uden, M.J.; de Vries, I.J.M.; Heerschap, A. Cell tracking using 19F magnetic resonance imaging: Technical aspects and challenges towards clinical applications. *European Radiology* **2015**, *25*, 726-735, doi:10.1007/s00330-014-3474-5.
19. Janjic, J.M.; Ahrens, E.T. Fluorine-containing nanoemulsions for MRI cell tracking. *Wiley Interdisciplinary Reviews: Nanomedicine and Nanobiotechnology* **2009**, *1*, 492-501, doi:10.1002/wnan.35.
20. Bourouina, N.; de Kort, D.W.; Hoeben, F.J.M.; Janssen, H.M.; Van As, H.; Hohlbein, J.; van Duynhoven, J.P.M.; Kleijn, J.M. Complex Coacervate Core Micelles with Spectroscopic Labels for Diffusometric Probing of Biopolymer Networks. *Langmuir* **2015**, *31*, 12635-12643, doi:10.1021/acs.langmuir.5b03496.
21. Pourcelle, V.; Laurent, S.; Welle, A.; Vriamont, N.; Stanicki, D.; Vander Elst, L.; Muller, R.N.; Marchand-Brynaert, J. Functionalization of the PEG Corona of Nanoparticles by Clip Photochemistry in Water: Application to the Grafting of RGD Ligands on PEGylated USPIO Imaging Agent. *Bioconjugate Chemistry* **2015**, *26*, 822-829, doi:10.1021/acs.bioconjchem.5b00041.
22. Zieringer, M.; Wyszogrodzka, M.; Biskup, K.; Haag, R. Supramolecular behavior of fluorous polyglycerol dendrons and polyglycerol dendrimers with perfluorinated shells in water. *New Journal of Chemistry* **2012**, *36*, 402-406, doi:10.1039/C1NJ20741E.
23. Li, S.; Yuan, Y.; Yang, Y.; Li, C.; McMahon, M.T.; Liu, M.; Chen, S.; Zhou, X. Potential detection of cancer with fluorinated silicon nanoparticles in 19F MR and fluorescence imaging. *Journal of Materials Chemistry B* **2018**, *6*, 4293-4300, doi:10.1039/C8TB00648B.
24. Rolfe, B.E.; Blakey, I.; Squires, O.; Peng, H.; Boase, N.R.B.; Alexander, C.; Parsons, P.G.; Boyle, G.M.; Whittaker, A.K.; Thurecht, K.J. Multimodal Polymer Nanoparticles with Combined 19F Magnetic Resonance and Optical Detection for Tunable, Targeted, Multimodal Imaging in Vivo. *Journal of the American Chemical Society* **2014**, *136*, 2413-2419, doi:10.1021/ja410351h.
25. Dichiarante, V.; Tirotta, I.; Catalano, L.; Terraneo, G.; Raffaini, G.; Chierotti, M.R.; Gobetto, R.; Baldelli Bombelli, F.; Metrangolo, P. Superfluorinated and NIR-luminescent gold nanoclusters. *Chemical Communications* **2017**, *53*, 621-624, doi:10.1039/C6CC09324H.
26. Zhang, L.; Li, Y.; Zhang, C.; Wang, Y.; Song, C. Pharmacokinetics and tolerance study of intravitreal injection of dexamethasone-loaded nanoparticles in rabbits. *Int J Nanomedicine* **2009**, *4*, 175-183, doi:https://doi.org/10.2147/IJN.S6428.
27. Miron, D.S.; Soldattelli, C.; Schapoval, E.E.S. HPLC with Diode-Array Detection for Determination of Leflunomide in Tablets. *Chromatographia* **2006**, *63*, 283-287, doi:10.1365/s10337-006-0739-4.
28. Yoo, H.S.; Park, T.G. Folate receptor targeted biodegradable polymeric doxorubicin micelles. *Journal of Controlled Release* **2004**, *96*, 273-283, doi:https://doi.org/10.1016/j.jconrel.2004.02.003.
29. Mora-Huertas, C.E.; Fessi, H.; Elaissari, A. Polymer-based nanocapsules for drug delivery. *International Journal of Pharmaceutics* **2010**, *385*, 113-142, doi:https://doi.org/10.1016/j.ijpharm.2009.10.018.
30. Chorny, M.; Fishbein, I.; Danenberg, H.D.; Golomb, G. Lipophilic drug loaded nanospheres prepared by nanoprecipitation: effect of formulation variables on size, drug

recovery and release kinetics. *Journal of Controlled Release* **2002**, *83*, 389-400, doi:https://doi.org/10.1016/S0168-3659(02)00211-0.
31. Lince, F.; Marchisio, D.L.; Barresi, A.A. Strategies to control the particle size distribution of poly-ε-caprolactone nanoparticles for pharmaceutical applications. *Journal of Colloid and Interface Science* **2008**, *322*, 505-515, doi:https://doi.org/10.1016/j.jcis.2008.03.033.
32. D'Avila Carvalho Erbetta, C.; José Alves, R.; Magalhães Resende, J.; Fernando de Souza Freitas, R.; Geraldo de Sousa, R. Synthesis and Characterization of Poly(D,L-Lactide-co-Glycolide) Copolymer *Journal of Biomaterials and Nanobiotechnology* **2012**, *3*, 208-225, doi:10.4236/jbnb.2012.32027.
33. Boccalon, M.; Franchi, P.; Lucarini, M.; Delgado, J.J.; Sousa, F.; Stellacci, F.; Zucca, I.; Scotti, A.; Spreafico, R.; Pengo, P., et al. Gold nanoparticles protected by fluorinated ligands for 19F MRI. *Chemical Communications* **2013**, *49*, 8794-8796, doi:10.1039/C3CC44572K.
34. Swider, E.; Staal, A.H.J.; Koen van Riessen, N.; Jacobs, L.; White, P.B.; Fokkink, R.; Janssen, G.-J.; van Dinther, E.; Figdor, C.G.; de Vries, I.Jolanda M., et al. Design of triphasic poly(lactic-co-glycolic acid) nanoparticles containing a perfluorocarbon phase for biomedical applications. *RSC Advances* **2018**, *8*, 6460-6470, doi:10.1039/C7RA13062G.
35. Pigliacelli, C.; Maiolo, D.; Nonappa; Haataja, J.S.; Amenitsch, H.; Michelet, C.; Sánchez Moreno, P.; Tirotta, I.; Metrangolo, P.; Baldelli Bombelli, F. Efficient Encapsulation of Fluorinated Drugs in the Confined Space of Water-Dispersible Fluorous Supraparticles. *Angewandte Chemie* **2017**, *129*, 16404-16408, doi:10.1002/ange.201710230.
36. Hoshyar, N.; Gray, S.; Han, H.; Bao, G. The effect of nanoparticle size on in vivo pharmacokinetics and cellular interaction. *Nanomedicine* **2016**, *11*, 673-692, doi:10.2217/nnm.16.5.
37. Bruni, R.; Possenti, P.; Bordignon, C.; Li, M.; Ordanini, S.; Messa, P.; Rastaldi, M.P.; Cellesi, F. Ultrasmall polymeric nanocarriers for drug delivery to podocytes in kidney glomerulus. *Journal of Controlled Release* **2017**, *255*, 94-107, doi:https://doi.org/10.1016/j.jconrel.2017.04.005.
38. Colombo, C.; Li, M.; Watanabe, S.; Messa, P.; Edefonti, A.; Montini, G.; Moscatelli, D.; Rastaldi, M.P.; Cellesi, F. Polymer Nanoparticle Engineering for Podocyte Repair: From in Vitro Models to New Nanotherapeutics in Kidney Diseases. *ACS Omega* **2017**, *2*, 599-610, doi:10.1021/acsomega.6b00423.
39. Welsh, G.I.; Saleem, M.A. The podocyte cytoskeleton—key to a functioning glomerulus in health and disease. *Nature Reviews Nephrology* **2011**, *8*, 14, doi:10.1038/nrneph.2011.151.